HHS Public Access

Author manuscript

J Biomech. Author manuscript; available in PMC 2019 April 05.

Published in final edited form as:

J Biomech. 2018 March 21; 70: 88–95. doi:10.1016/j.jbiomech.2017.09.026.

Segmental variations in facet joint translations during *in vivo* lumbar extension

Ryan M. Byrne[a], **Yu Zhou**[e], **Liying Zheng**[c], **Suman K. Chowdhury**[e], **Ameet Aiyangar**[b,d,*], and **Xudong Zhang**[e,f,*]

[a] Department of Mechanical Engineering and Materials Science, University of Pittsburgh, Pittsburgh, PA 15203, USA [b] Department of Orthopaedic Surgery, University of Pittsburgh, Pittsburgh, PA 15203, USA [c] Health Effects Lab Division, National Institute for Occupational Safety and Health, Morgantown, WV 26505, USA [d] Mechanical Systems Engineering, EMPA (Swiss Federal Laboratories for Materials Science and Technology), 8600 Duebendorf, Switzerland [e] Department of Industrial & Systems Engineering, Texas A&M University, College Station, TX 77843, USA [f] Department of Mechanical Engineering, Texas A&M University, College Station, TX 77843, USA

Abstract

The lumbar facet joint (FJ) is often associated with pathogenesis in the spine, but quantification of normal FJ motion remains limited to *in vitro* studies or static imaging of non-functional poses. The purpose of this study was to quantify lumbar FJ kinematics in healthy individuals during functional activity with dynamic stereo radiography (DSX) imaging. Ten asymptomatic participants lifted three known weights starting from a trunk-flexed (~75°) position to an upright position while being imaged within the DSX system. High resolution computed tomography (CT) scan-derived 3D models of their lumbar vertebrae (L2-S1) were registered to the biplane 2D radiographs using a markerless model-based tracking technique providing instantaneous 3D vertebral kinematics throughout the lifting tasks. Effects of segment level and weight lifted were assessed using mixed-effect repeated measures ANOVA. Superior-inferior (SI) translation dominated FJ translation, with L5S1 showing significantly less translation magnitudes (*Median (Md) = 3.5 mm, $p < 0.0001$*) than L2L3, L3L4, and L4L5 segments *(Md = 5.9 mm, 6.3 mm and 6.6 mm respectively*). Linear regression-based slopes of continuous facet translations revealed strong linearity for SI translation ($r^2 > 0.94$), reasonably high linearity for sideways sliding (*Z*-) ($r^2 > 0.8$), but much less linearity for facet gap change (*X*-) ($r^2 \sim 0.5$). Caudal segments (L4-S1), particularly L5S1, displayed greater coupling compared to cranial (L2-L4) segments, revealing distinct differences overall in FJ translation trends at L5S1. No significant effect of weight lifted on FJ translations was detected. The study presents a hitherto unavailable and highly precise baseline dataset of facet translations measured during a functional, dynamic lifting task.

* Corresponding authors at: Mechanical Systems Engineering, EMPA (Swiss Federal Laboratories for Materials Science and Technology), 8600 Duebendorf, Switzerland (A. Aiyangar). 4077 Emerging Technologies Building, 3131 Texas A&M University, College Station, TX 77843-3131, USA (X. Zhang). ameet.aiyangar@empa.ch (A. Aiyangar), xudongzhang@tamu.edu (X. Zhang).

Conflict of interest statement

The authors hereby state that none of us has a potential conflict of interest (e.g. consultancies, stock ownership, equity interests, patent-licensing arrangements) related to the manuscript or the work it describes.

Keywords

Lumbar facet joint; *In vivo* facet translations; Dynamic stereo X-ray imaging; Lifting task; Segment-specific differences

1. Introduction

Lumbar facet joint (FJ) pain is a prevalent pathology shown to account for around 20% of cases of low-back pain (Friedrich et al., 2007; Manchukonda et al., 2007), but its biomechanical antecedents are less clear. Although changes in FJ mechanics, particularly kinematics, have been linked to tissue degeneration (Boswell et al., 2003; Simon et al., 2012; Vernon-Roberts and Pirie, 1977), quantification of their normal mechanics *in vivo* during functional activity is lacking. Such normative data are important, as studies have alluded to associations between deviations from "*normal*" facet mechanics and the overloading or damaging of surrounding spinal tissues, such as facet cartilage, capsular tissues, and intervertebral discs (Fujiwara et al., 2000; Li et al., 2011; Simon et al., 2012). Additionally, excessive or *abnormal* motion between lumbar facet surfaces can cause nerve compression and stress the well-innervated cartilaginous tissues and capsular ligaments of the FJ, which have been shown to release pain receptors when put under significant stress (Cavanaugh et al., 1996a; Igarashi et al., 2004; Lu et al., 2005b; Yamashita et al., 1996a,b).

From a clinical perspective, an accurate depiction of normal facet joint *translational kinematics* can help improve our understanding as well as diagnoses of degenerative diseases such as FJ osteoarthritis. For example, FJ space is an important metric for evaluating the progression of osteoarthritis, as narrowing of the facet gap and subsequent articular cartilage thinning have been highly correlated with the onset of osteoarthritis (Buckland-Wright, 2004; Pathria et al., 1987; Simon et al., 2012). Nevertheless, static CT imaging-based evaluations of facet gap (Simon et al., 2012) or facet contact area (Otsuka et al., 2010) may not discern the presence of different damage mechanisms based on differing movement patterns (Adams and Hutton, 1983), and, as reiterated by Simon et al. (2012), relationships between extent and location of facet degeneration and *in vivo* kinematics still require further clarification. Secondly, although FJ pain and associated osteoarthritic conditions are often preceded by degenerative disc disease, it has also been shown to occur without concomitant disc degeneration in about 20% of degenerated spines (Videman et al., 1995). This implies FJ pathologies are not always directly attributable to pathologies arising within the intervertebral disc (Kalichman and Hunter, 2007; Lewin, 1964; Swanepoel et al., 1995; Videman et al., 1995).

Quantifying dynamic *in vivo* lumbar FJ motion, however, can be quite challenging given the relatively small magnitudes of translation. Currently, our understanding of FJ motion is based primarily on cadaveric studies (Adams and Hutton, 1983; Stokes, 1988) or CT and MRI imaging in static, non-functional positions (Simon et al., 2012; Svedmark et al., 2015; Svedmark et al., 2012). Li and co-workers were the first — and to our knowledge, the only group — to demonstrate the use of biplane video-fluoroscopic imaging to quantify lumbar facet 3D angular and translational orientations in static, functional weight-bearing poses in

healthy individuals (Kozanek et al., 2009). While their study provided invaluable insight into FJ orientation in static poses, a dynamic dataset acquired during functional activities could offer more clarity regarding normal physiological motion of the lumbar facet joints.

Hence, the purpose of this study was to quantify 3D, bilateral functional lumbar FJ kinematics in healthy individuals. We used a previously acquired dynamic dataset of lumbar vertebral motion during a functional, dynamic lifting task (Aiyangar et al., 2015, 2017, 2014). Since measures of facet gap and facet sliding are the most relevant metrics for clinical applications, we focused on the translational characteristics of the lumbar facet joint kinematics in this study. We hypothesized that facet translation would vary across individual lumbar (L2-S1) segments as well as with magnitude of external load lifted.

2. Methods

2.1. Experimental data acquisition

In an institutional review board (IRB)-approved study, 14 healthy participants (ages 19–30) reporting no history of low back disorders were recruited. After providing written consent, participants completed a series of lifting tasks (two trials for each of three different weights: 4.5 kg, 9.1 kg and 13.6 kg) in a sagittally symmetric motion without bending their knees. Participants started from an approximately 75° trunk-flexed position (~44° L2-S1 flexion) (Aiyangar et al., 2015) until reaching an upright position. Additionally, static standing trials with the subject holding no weight were performed. Adequate rest was provided between trials.

During each trial, the DSX system recorded dynamic X-ray images of the participants' lumbar spine in the sagittal and frontal planes at 30 frames per second (fps) for two seconds (pulsed exposure = 4 ms/frame, excitation voltage = 70–80 kV, current = 320–630 mA, effective radiation dose per dynamic trial <0.6 mSv). High resolution computed tomography (CT) scans (voxel size = 0.25 mm × 0.25 mm × 1.25 mm, effective radiation dose <12.3 mSv) of each participant's lumbar spine were also obtained, from which individual vertebrae would be segmented to create 3D bone models using Mimics 14.0 (Materialise Inc., Ann Arbor, MI). The instantaneous 3D position of each vertebra was then determined by registering the 3D CT-based bone models to the 2D DSX radiographs for every recorded frame using a previously validated semi-automated markerless model-based tracking process (precision ≤ 0.2 mm and 0.26°) (Lee, 2010). More details on the experimental data acquisition can be seen in a series of prior publications (Aiyangar et al., 2015, 2017, 2014).

2.2. Kinematics analysis

Due to image quality and capture volume limits, L1 kinematics could not be included in this study. Local coordinate systems (LCS), based on four landmarks points (inferior, superior, posterior, and anterior), were defined on the inner and outer surfaces of the superior and inferior facets, respectively, of each vertebra from the L2 to S1 (Fig. 1). The average location of the four landmarks defined the LCS origin. The *Z*-axis represented the direction parallel to the facet faces *(sideways facet sliding)*. The *X*-axis represented the direction normal to the facet faces *(facet gap.)* The Y-axis represented the superior-inferior direction, creating a

right-handed orthogonal coordinate system on both the left and right facet surfaces. Body-fixed translations of the lower facet LCS of the superior vertebra with respect to the upper facet LCS of the inferior vertebra (left and right) were calculated for all static and dynamic trials. At each time frame, from the start to completion of the lift, the change in *X*-, *Y*-, and *Z*- body-fixed translations with respect to the fully flexed body-fixed translations were reported. Differences between the instantaneous body-fixed translations of the flexed and static upright positions were also reported. To consistently describe facet joint kinematics between left and right facet joints, a positive translation along the *X*-axis of the inferior vertebra's upper facet LCS represented an increase in facet gap, whereas a negative translation represented a decrease in facet gap. Data were presented with respect to progression of the lift, or percent task completion ($PTC = \frac{\theta_c - \theta_i}{\theta_f - \theta_i} \times 100$; θ_c, θ_i, θ_f = current, initial and final L2-S1 angle respectively), as opposed to time. PTC is a normalization of time based on overall L2-S1 flexion angle, with 0% and 100% corresponding to the start (fully-flexed) and end (upright reference) position, respectively.

2.3. Statistical analysis

Data acquired from the two trials per task were averaged into a single dataset. Further, results from the left and right FJ were not significantly different (except for *X*- component of L2L3 and L3L4 segments); hence these data were averaged. Data from three participants were excluded owing to poor image capture quality and tracking issues. One additional participant was excluded due to poor image quality for the static trials making 10 participants' data available for processing yielding 116 observations. Mean ($\pm CI_{95}$) translations in the *X*-, *Y*- and *Z* directions for every decile of L2-S1 extension range-of-motion (ROM) were computed for each load-lifting task across participants to enable qualitative observations of differences across segments and across load levels. Time series plots ("time" as indicated by PTC) of the translations between 0% and 80% of L2-S1 ROM were generated, with the start of the lift (fully flexed position) defined as our zero-translation reference position. Corresponding linear regression-based slopes were computed to identify migration trends, demonstrated by a slope significantly different from zero ($\alpha = 0.05$).

Repeated measures analysis was employed with data compiled as a mixed model, with segmental level (four levels: L2L3, L3L4, L4L5, L5S1) and load magnitude [three levels: 4.54 kg (10 lb), 9.1 kg (20 lb), 13.6 kg (30 lb)] as the two within-subject, fixed effect, categorical factors and "participant" as the random factor. The total translations in each of the three directions were the outcome variables. Differences across segments and load magnitudes were assessed based on post-hoc Tukey's Honest Significant Difference (HSD) comparison-of-means tests. Similar analyses were also conducted for left and right facet X-translation components separately. The extent of overlap between the notches of respective boxes in notched box plots (Mcgill et al., 1978; R_Core_Team, 2015) of the left-right averaged datasets provided an additional, visual representation of the differences between the groups. The notches, which represent a 95% confidence interval (CI_{notch}) of the median, extend to $[\pm 1.58 * IQR/((n)^{0.5})]$, where "IQR" = interquartile range between first to third quartile, and "n" = number of non-missing observations within the group. No overlap

indicated significant differences. All analyses were performed in R® statistical computing software (R_Core_Team, 2015).

3. Results

Static, upright (reference) SI spacing was substantially larger at L5S1 compared to other segments (Table 1). Although coupled translation was observed, translation in the superior-inferior (SI, local *Y*-axis) direction was the dominant contributor. SI translation was significantly lower in L5S1 *[$p < 0.001$]* compared to L2L3, L3L4 and L4L5 segments. No significant differences were detected between the other segments ($p > 0.5$, Fig. 2, Table 2). L4L5 and L5S1 exhibited larger translations along the averaged, local *X*- *[Median (Md) = 0.4 mm and 0.4 mm, respectively]* and *Z*-axes *(Md = −1.5 mm and −1.6 mm, respectively)* compared to L2L3 and L3L4 *[(x-axis Md = 0.2 mm and 0.03 mm, respectively; z-axis Md = −0.7 mm and −0.7 mm, respectively]*. Following differences were significant along *Z*- (L5S1 > L3L4, $p = 0.01$; L4L5 > L3L4, $p = 0.04$, L5S1 > L2L3, $p < 0.001$; L4L5 > L2L3, $p = 0.0016$). For the right side, L5S1 and L4L5 *X*-components were significantly greater than L3L4 ($p = 0.01$ and 0.04 respectively). Averaged *X*-component translations as well as those for the left facets were not significantly different across segments. Time series plots including the mean ($\pm CI_{95}$) for the segment-specific translations for each of the three load cases are shown in Fig. 3. Corresponding linear regression-based slopes (Fig. 4) revealed strong linearity ($r^2 > 0.94$) for SI translation component and reasonably good linear fit for the sideways sliding (*Z*-) component ($r^2 > 0.8$), with a much lower correlation coefficient for *X*-component (facet gap, $r^2 \sim 0.5$). No significant effect of the magnitude of weight lifted was detected ($p > 0.7$, Fig. 5, Table 3). Overall magnitudes of translation in the superior (L2-L5) segments were quite similar *[Md ($\pm CI_{notch}$) = 5.9 (±0.7) mm, 6.6(±0.6) mm and 6.9(±0.6) mm respectively]*, but L5S1 facet translations were markedly different *(Md = 4.1mm, $p < 0.0001$)*. Statistical tests showed no significant differences in left-right averaged *facet gap* translation between segments, but greater translation was indicated at the caudal segments (L4L5 and L5S1) than at the cranial segments (L2L3 and L3L4) (Fig. 2). Moreover, they were significantly different from zero, based on the confidence intervals of the notched box plots. Similar inferences could be made regarding the facet-sliding component, although translations in the caudal segments were clearly significantly larger than the cranial segments. The continuous time-series curves (Fig. 3) generally confirmed this trend, at least for sideways facet sliding: *Z*-translation appeared to be greater (more negative) at the caudal segments. Trends in *X*-translations (*facet gap*) were less apparent across all the trials.

4. Discussion

4.1. Segment-specific differences

The clearest differences were observed in SI translation, which was about 45% less at L5S1 compared to the rest, on average. The highly linear time-series curves (Fig. 4b) imply that, at least for healthy and asymptomatic individuals, accurate end-ROM based measurements at flexed and upright poses *might* be adequate to estimate SI translations within the lumbar facet joints. However, comparing SI translation results with the limited number of previous

studies based on end-ROM static imaging techniques yields somewhat mixed results. For example, (Svedmark et al., 2012) reported overall translation magnitudes of 6.5 mm and 4.6 mm at the L4L5 and L5S1 facets respectively, although these were based on CT measurements of supine flexed- and extended spines. On the other hand, (Kozanek et al., 2009) reported L4L5 translations to be much lower than L2L3 and L3L4 segments. Moreover, the overall magnitudes reported were also much lower ($\bar{x} < 4\ mm$) than those measured in the current study.

Interestingly, although SI *translations* at the L5S1 facets were of a smaller magnitude, SI FJ *spacing* at the static upright position was considerably larger compared to the other segments (Table 1). A possible explanation could be that in the standing position, there is an inherent superior shift in FJ spacing at L5S1 compared to other segments on account of a difference in vertebral orientation and lordosis. Although the SI spacing is approximately 2 mm larger for L5S1 in upright stance compared to the upper segments, it should necessarily reduce further in hyperextension, when the facet joints bear a larger proportion of the lumbar loads, with the magnitude of translation being proportionally larger in L5S1. Orientation and translation patterns also suggest greater contact forces and hence higher risk of wear at the lower extremities of the superior (L5) facets; however few studies are available to directly confirm this hypothesis. FE models of functional spinal units simulating sagittal rotation have predicted greater contact at relatively superior locations on the inferior facet of the superior bone (L2) for the L2-L3 joint (Shirazi-Adl, 1991) but relatively more inferior locations on L4 inferior facets for the L4-L5 joint (Schmidt et al., 2008), implying a progressive downward shift of the contact location from cranial to caudal segments. Secondly, the combination of a larger SI spacing along with a smaller *facet gap* for L5S1 facets, which narrows further into a flexion pose, also suggests upper extremities of the S1 facet could be at higher risk for wear and degeneration, particularly with any disc height loss following an onset of disc degenerative conditions. Results from a recent FE study (Du et al., 2016) appear consistent with this hypothesis: contact forces during flexion movement appeared exclusively in the L5S1 segment on the upper extremities of the superior facets of S1. Facet contact did not appear to occur within the upper (L1-L5) segments during flexion.

Translations in *X*- (*facet gap* normal to facet face) and *Z*- (facet sliding parallel to facet face) directions were relatively small and similar to those reported by (Kozanek et al., 2009). The results indicate that coupled translation patterns in the caudal segments, while small, are significant, particularly for L5S1. Some of the segment-wise differences in *X*- and *Z*-directions could be due to differences in articular facet orientation. (Masharawi et al., 2004) reported progressively more coronally oriented facet surfaces as one moved caudally along the thoracolumbar spine, postulating this to be an adaptation to allow a progressively increased range of movement in the lumbar segments. Masharawi et al. also showed that the mismatch in both transverse orientation (angle made with the sagittal plane) and longitudinal orientation (angle made with the frontal plane) between the adjacent facets increased from the cranial to the caudal segments. This “opening up” of facet surfaces in the two directions could explain the larger changes in *facet gap* and *facet sliding* observed at the caudal segments in the current study, further supporting Masharawi et al.’s speculation that a mismatch in orientation of adjacent facets encourages more coupled translations.

One peculiarity in the results was the difference in *X*- (facet gap) translation magnitudes between left- and right sides for L2L3 and L3L4. Our previous analyses on vertebral 3D rotations did show coupled, non-sagittal translations and rotations to be small, but significantly greater than zero (Aiyangar et al., 2014). Although differences were not statistically significant, cranial segments exhibited slightly larger lateral bending (Table 4), which might partially explain these differences by simultaneously increasing *facet gap* on one side while reducing it proportionally on the other.

4.2. Load-specific differences

No significant differences in facet translations were observed due to magnitude of the lifted load. Previous investigations into effect of the external load on intervertebral rotations patterns and migration patterns of the instantaneous centers of rotation based on this dataset also failed to discern statistically significant differences (Aiyangar et al., 2015, 2017). However, this does not necessarily imply that external weight does not have any effect on FJ motion. It is plausible that the incremental increase in load for this study was not enough to produce significant effects on lumbar facet kinematics.

4.3. Implications for facet-based pain

The study presents a hitherto unavailable baseline dataset of facet translations measured accurately and with high precision during dynamic, functional activities. The primary motivation for documenting a benchmark for FJ translations in a healthy cohort, however, was to enable future investigations of the biomechanical antecedents of pathological conditions. It is then worthwhile to ponder the implications of deviations from the relatively small translations observed in this study.

Although motion between facet surfaces is relatively small, nominal strains developed within the facet capsules during the course of a normal range of motion can be quite large. For example, Ianuzzi et al. (2004) demonstrated that principle strains in the facet capsules reached upwards of 14% for a prescribed lumbar flexion angle (40°). *In vitro* studies have suggested the strain threshold for sustained painful capsular stretching to be anywhere from 20% to 47% (Dong et al., 2008; Dong and Winkelstein, 2010; Jaumard et al., 2011; Lee et al., 2004; Lu et al., 2005a,b). Relatively minor increases in translation — of the order of a millimeter — could significantly increase capsular strains and consequently the likelihood of pain, particularly if these translations were sustained or occurred repeatedly during daily activity. Secondly, small deviations from the normal ranges of translation could increase the risk of adjoining facet face impingement and surface cartilage wear. For example, observations of facet kinematics in patients with DDD revealed a marked increase in coupling of the translation components compared to asymptomatic controls (Li et al., 2011). These increases were observed at the index- as well as the adjacent level. The situation could be particularly exacerbated in conditions associated with lumbar instability, where sudden but transient deviations in translation patterns could momentarily cause impingement within the facet joints, or cause facet capsular strain levels to exceed the pain threshold. Further studies are needed to quantify the threshold for kinematic deviations leading to the onset of painful FJ pathological conditions.

Several limitations are present within this study. First, a few participants' data were not useable, reducing the sample size of our study to 10. Additionally, we were unable to include the L1 in our study due to capture volume limitations of the DSX system. The age range of participants included in this study was very limited as well and is not representative of the general demographics. However, since our goal was to provide a dataset of healthy lumbar kinematics, the relatively young age group included in this study may be adequate. Although all participants were instructed and trained to finish the lifting motion within a 2-second time period, not all participants were able to reach their upright position (100% PTC) during DSX imaging, limiting our ability to quantify lumbar facet motion at time instances exceeding 80% PTC.

Acknowledgements

The work was funded by a research grant (R21OH00996) from the Centers for Disease Control and Prevention/ National Institute for Occupational Safety and Health (CDC/NIOSH). Additional support was received through the *Ambizione* Career Grant Award (PZ00P2_154855/1) from the Swiss National Science Foundation (SNSF). The authors thank Dr. William Anderst for technical advice on post-processing of the data acquired from the DSX system.

References

Adams MA, Hutton WC, 1983 The mechanical function of the lumbar apophyseal joints. Spine 8, 327–330. [PubMed: 6623200]

Aiyangar A, Zheng L, Anderst W, Zhang X, 2015 Apportionment of lumbar L2– S1 rotation across individual motion segments during a dynamic lifting task. J. Biomech 48, 3718–3724.

Aiyangar A, Zheng L, Anderst W, Zhang X, 2017 Instantaneous centers of rotation for lumbar segmental extension in vivo. J. Biomech 52, 113–121. [PubMed: 28062121]

Aiyangar AK, Zheng LY, Tashman S, Anderst WJ, Zhang XD, 2014 Capturing three-dimensional in vivo lumbar intervertebral joint kinematics using dynamic stereo-X-ray imaging. J. Biomech. Eng.-T. ASME 136, 011004.

Boswell MV, Singh V, Staats PS, Hirsch JA, 2003 Accuracy of precision diagnostic blocks in the diagnosis of chronic spinal pain of facet or zygapophysial joint origin. Pain Phys. 6, 449–456.

Buckland-Wright C, 2004 Subchondral bone changes in hand and knee osteoarthritis detected by radiography. Osteoarthritis Cartilage 12 Suppl A, S10–19. [PubMed: 14698636]

Cavanaugh J, Ozaktay CA, Yamashita T, King AI, 1996a Lumbar facet pain: biomechanics, neuroanatomy and neurophysiology. J. Biomech 29, 1117–1129. [PubMed: 8872268]

Dong L, Odeleye AO, Jordan-Sciutto KL, Winkelstein BA, 2008 Painful facet joint injury induces neuronal stress activation in the DRG: implications for cellular mechanisms of pain. Neurosci. Lett 443, 90–94. [PubMed: 18675314]

Dong L, Winkelstein BA, 2010 Simulated whiplash modulates expression of the glutamatergic system in the spinal cord suggesting spinal plasticity is associated with painful dynamic cervical facet loading. J. Neurotrauma 27, 163–174. [PubMed: 19772459]

Du CF, Yang N, Guo JC, Huang YP, Zhang C, 2016 Biomechanical response of lumbar facet joints under follower preload: a finite element study. BMC Musculoskelet Disord. 17, 126. [PubMed: 26980002]

Friedrich KM, Nemec S, Peloschek P, Pinker K, Weber M, Trattnig S, 2007 The prevalence of lumbar facet joint edema in patients with low back pain. Skeletal. Radiol 36, 755–760. [PubMed: 17410353]

Fujiwara A, Tamai K, An HS, Kurihashi T, Lim TH, Yoshida H, Saotome K, 2000 The relationship between disc degeneration, facet joint osteoarthritis, and stability of the degenerative lumbar spine. J. Spinal Disord 13, 444–450. [PubMed: 11052356]

Ianuzzi A, Little JS, Chiu JB, Baitner A, Kawchuck G, Khalsa PS, 2004 Human lumbar facet joint capsule strains: I. During physiological motions. Spine J. 4, 141–152. [PubMed: 15016391]

Igarashi A, Kikuchi S, Konno S, Olmarker K, 2004 Inflammatory cytokines released from the facet joint tissue in degenerative lumbar spinal disorders. Spine 29, 2091–2095. [PubMed: 15454697]

Jaumard NV, Welch WC, Winkelstein BA, 2011 Spinal facet joint biomechanics and mechanotransduction in normal, injury and degenerative conditions. J. Biomech. Eng 133, 071010. [PubMed: 21823749]

Kalichman L, Hunter DJ, 2007 Lumbar facet joint osteoarthritis: a review. Semin. Arthritis. Rheum 37, 69–80. [PubMed: 17379279]

Kozanek M, Wang S, Passias PG, Xia Q, Li G, Bono CM, Wood KB, Li G, 2009 Range of motion and orientation of the lumbar facet joints in vivo. Spine (Phila Pa 1976) 34, E689–696. [PubMed: 19730201]

Lee JBE, Anderst WJ, 2010 Lumbar spine motion during functional movement: in vivo validation of flexion/extension movement tracking. In: 3rd Annual Lumbar Spine ResearchSociety Meeting, Chicago, IL, USA.

Lee KE, Davis MB, Mejilla RM, Winkelstein BA, 2004 In vivo cervical facet capsule distraction: mechanical implications for whiplash and neck pain. Stapp. Car Crash. J 48, 373–395. [PubMed: 17230274]

Lewin T, 1964 Osteoarthritis in lumbar synovial joints. A morphologic study. Acta Orthop. Scand. Suppl, SUPPL 73, 71–112.

Li W, Wang S, Xia Q, Passias P, Kozanek M, Wood K, Li G, 2011 Lumbar facet joint motion in patients with degenerative disc disease at affected and adjacent levels: an in vivo biomechanical study. Spine (Phila Pa 1976) 36, E629–637. [PubMed: 21270686]

Lu Y, Chen C, Kallakuri S, Patwardhan A, Cavanaugh JM, 2005a Development of an in vivo method to investigate biomechanical and neurophysiological properties of spine facet joint capsules. European Spine J.: Official Publ. Eur. Spine Soc., Eur. Spinal Deformity Soc., Eur. Section Cervical Spine Res. Soc 14, 565–572.

Lu Y, Chen C, Kallakuri S, Patwardhan A, Cavanaugh JM, 2005b Neural response of cervical facet joint capsule to stretch: a study of whiplash pain mechanism. Stapp. Car Crash. J 49, 49–65. [PubMed: 17096268]

Manchukonda R, Manchikanti KN, Cash KA, Pampati V, Manchikanti L, 2007 Facet joint pain in chronic spinal pain: an evaluation of prevalence and falsepositive rate of diagnostic blocks. J. Spinal Disord. Tech. 20, 539–545. [PubMed: 17912133]

Masharawi Y, Rothschild B, Dar G, Peleg S, Robinson D, Been E, Hershkovitz I, 2004 Facet orientation in the thoracolumbar spine: three-dimensional anatomic and biomechanical analysis. Spine (Phila Pa 1976) 29, 1755–1763. [PubMed: 15303019]

Mcgill R, Tukey JW, Larsen WA, 1978 Variations of box plots. Am. Stat 32, 12–16.

Otsuka Y, An HS, Ochia RS, Andersson GB, Espinoza Orias AA, Inoue N, 2010 In vivo measurement of lumbar facet joint area in asymptomatic and chronic low back pain subjects. Spine (Phila Pa 1976) 35, 924–928. [PubMed: 20354471]

Pathria M, Sartoris DJ, Resnick D, 1987 Osteoarthritis of the facet joints: accuracy of oblique radiographic assessment. Radiology 164, 227–230. [PubMed: 3588910]

R_Core_Team, 2015 R: A Language and Environment for Statistical Computing. R Foundation for Statistical Computing, Vienna, Austria.

Schmidt H, Heuer F, Claes L, Wilke HJ, 2008 The relation between the instantaneous center of rotation and facet joint forces - A finite element analysis. Clin. Biomech. (Bristol, Avon) 23, 270–278.

Shirazi-Adl A, 1991 Finite-element evaluation of contact loads on facets of an L2-L3 lumbar segment in complex loads. Spine (Phila Pa 1976) 16, 533–541. [PubMed: 2052996]

Simon P, Espinoza Orias AA, Andersson GB, An HS, Inoue N, 2012 In vivo topographic analysis of lumbar facet joint space width distribution in healthy and symptomatic subjects. Spine (Phila Pa 1976) 37, 1058–1064. [PubMed: 22433501]

Stokes IA, 1988 Mechanical function of facet joints in the lumbar spine. Clin. Biomech 3, 101–105.

Svedmark P, Berg S, Noz ME, Maguire GQ, Jr., Zeleznik MP, Weidenhielm L, Nemeth G, Olivecrona H, 2015 A new CT method for assessing 3D movements in lumbar facet joints and vertebrae in patients before and after TDR. Biomed. Res. Int 2015, 260703. [PubMed: 26587533]

Svedmark P, Tullberg T, Noz ME, Maguire GQ, Jr., Zeleznik MP, Weidenhielm L, Nemeth G, Olivecrona H, 2012 Three-dimensional movements of the lumbar spine facet joints and segmental movements: in vivo examinations of normal subjects with a new non-invasive method. Eur. Spine J 21, 599–605. [PubMed: 21881866]

Swanepoel MW, Adams LM, Smeathers JE, 1995 Human lumbar apophyseal joint damage and intervertebral disc degeneration. Ann. Rheum. Dis 54, 182–188. [PubMed: 7748015]

Vernon-Roberts B, Pirie CJ, 1977 Degenerative changes in the intervertebral discs of the lumbar spine and their sequelae. Rheumatol. Rehabil 16, 13–21. [PubMed: 847320]

Videman T, Battie MC, Gill K, Manninen H, Gibbons LE, Fisher LD, 1995 Magnetic resonance imaging findings and their relationships in the thoracic and lumbar spine. Insights into the etiopathogenesis of spinal degeneration. Spine (Phila Pa 1976) 20, 928–935. [PubMed: 7644958]

Yamashita T, Minaki Y, Ã–zaktay CN, Cavanaugh J, King AI, 1996 A morphological study of the fibrous capsule of the human lumbar facet joint. Spine 21, 538–543. [PubMed: 8852306]

Yamashita T, Minaki Y, Ozaktay AC, Cavanaugh JM, King AI, 1996 A morphological study of the fibrous capsule of the human lumbar facet joint. Spine (Phila Pa 1976) 21, 538–543. [PubMed: 8852306]

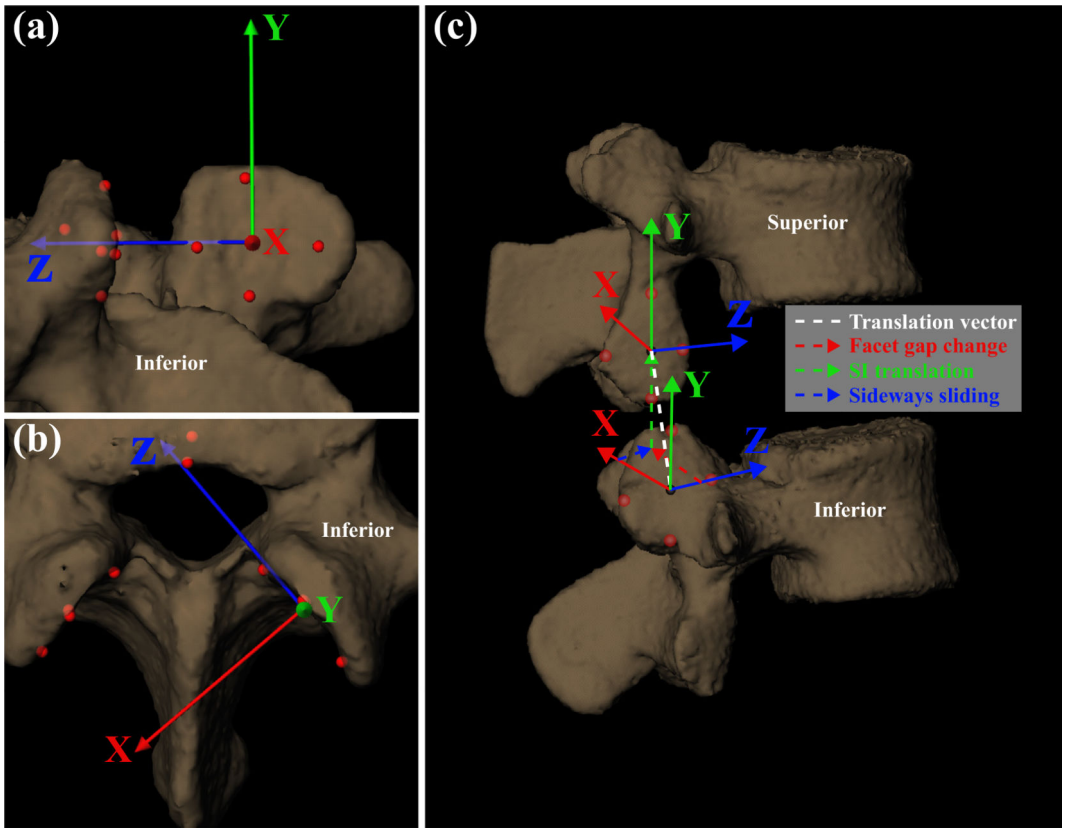

Fig. 1.

Local coordinate systems (LCS) on the inferior and superior facet surfaces. Depicted translations have been exaggerated for clarity. (a) Viewing direction normal to surface of superior facet of inferior vertebra, (b) viewing direction nominally superior to the facet surface, and (c) view displaying the superior and inferior vertebrae of a given lumbar intervertebral segment.

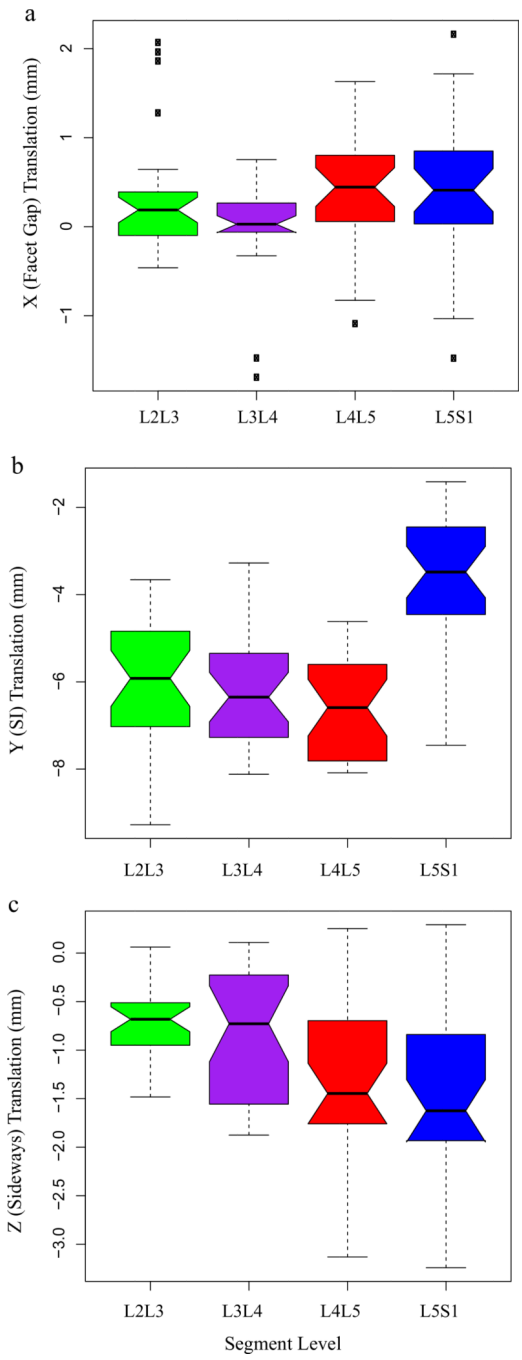

Fig. 2.

Effect of segment level on facet translation. (a) *X*-direction or facet gap, (b) *Y*-direction or superior-inferior translation, and (c) *Z*-direction or sideways sliding. Notches indicate confidence intervals of the median. Lack of overlap between notches indicates significant difference. Plot whiskers encompass the total range of data in each group.

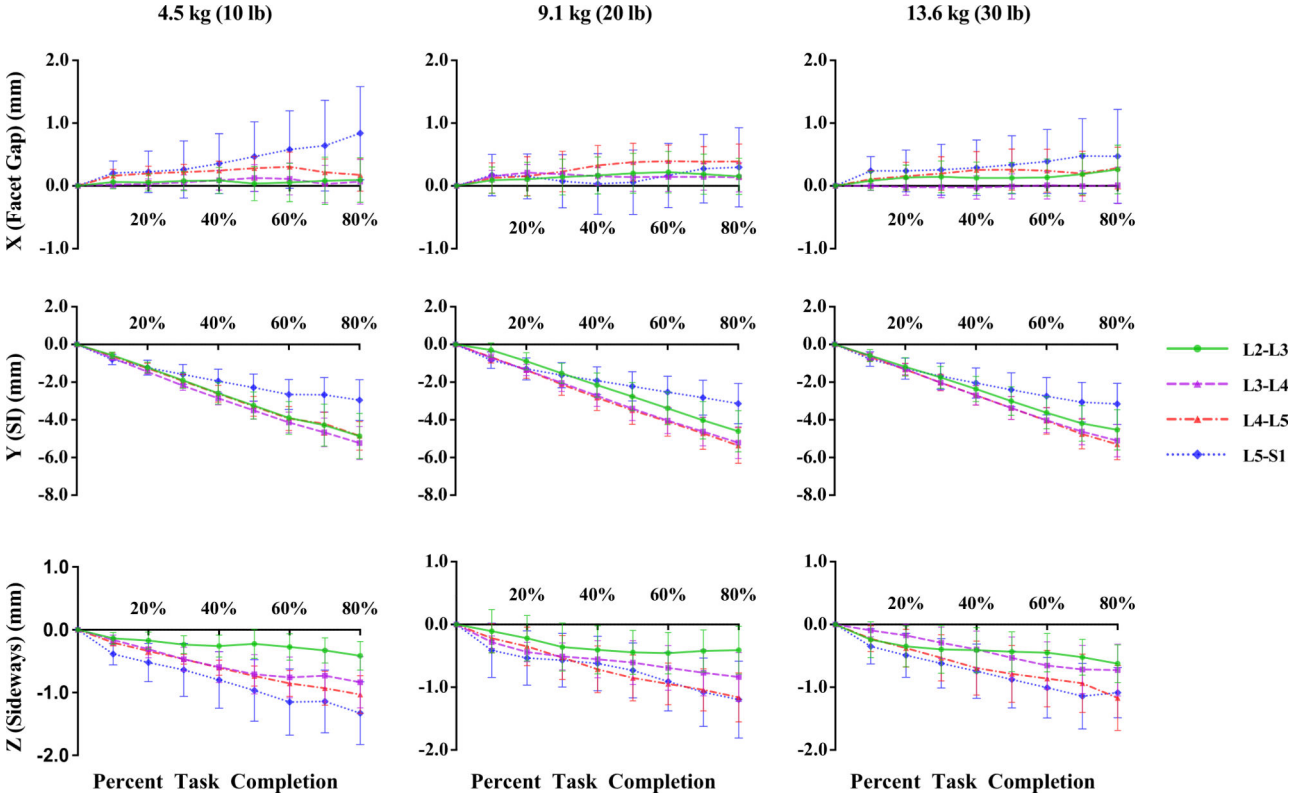

Fig. 3.

Lumbar facet translations in the *X*-, *Y*-, and *Z*-directions from the starting flexed position to 80% percent task completion – flexed position being the zero point. Error bars represent ±95% confidence intervals.

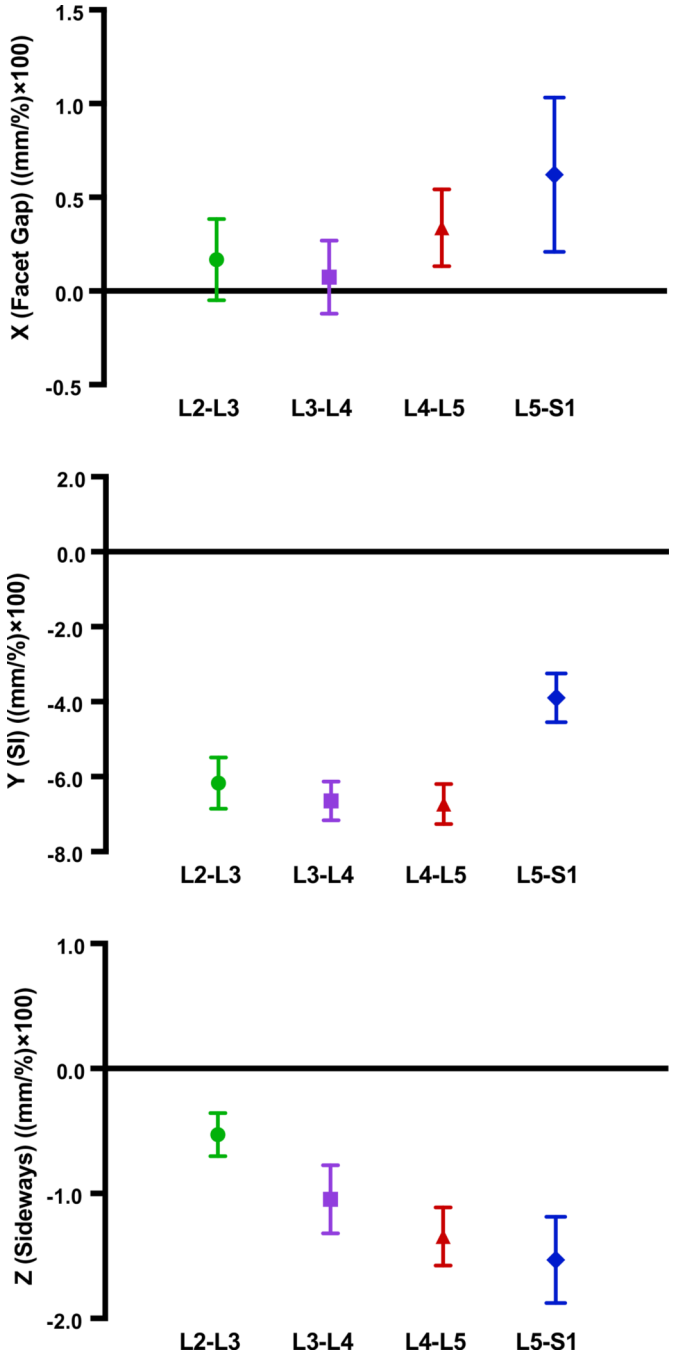

Fig. 4.

Linear regression-based slopes of the facet joint translation components for each segment. (a) *X*-direction of facet gap, (b) *Y*-direction or superior-inferior translation, and (c) *Z*-direction or sideways sliding. Units are (mm/%), but values are scaled (×100) for clarity of display. Error bars indicate ±95% confidence intervals. Lack of overlap between error bars between groups indicates significant difference.

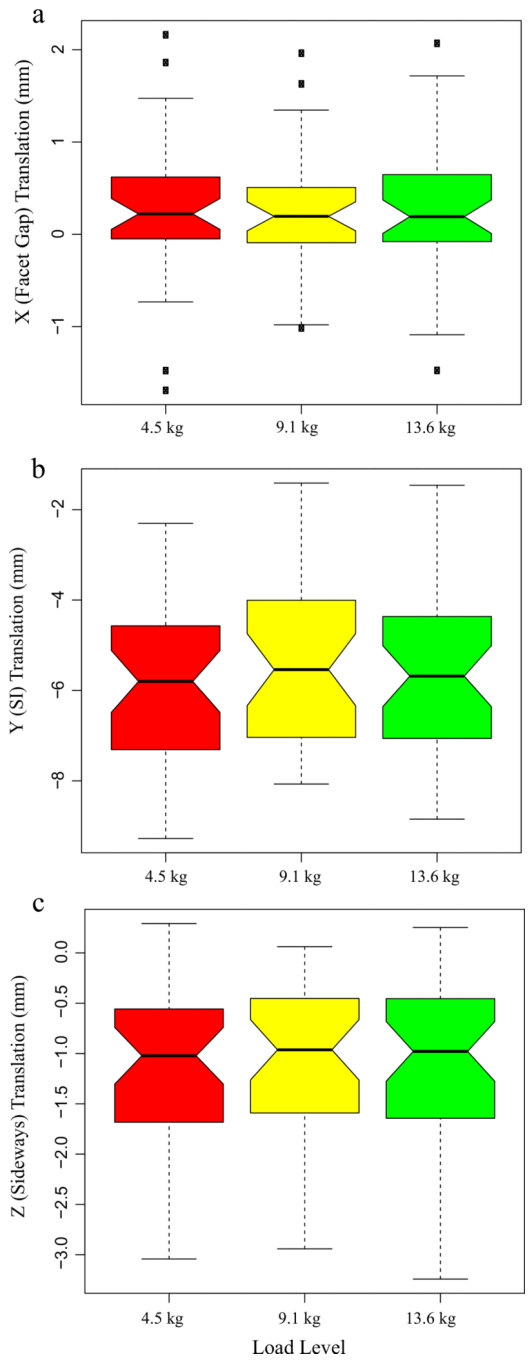

Fig. 5.

Effect of load magnitude on facet translation: (a) *X*-direction or facet gap, (b) *Y*-direction or superior-inferior direction, and (c) *Z*-direction or sideways sliding. Notches indicate confidence intervals of the median. Lack of overlap between notches indicates significant difference. Plot whiskers encompass the total range of data in each group.

Table 1

Segment-specific facet joint translations at the upright standing position. Values are Mean and 95% Confidence Intervals $\left(\bar{x} \pm CI_{95}\right)$.

	(a) *X* (facet gap) (mm)			(b) *Y* (SI sliding) (mm)			(c) *Z* (sideways sliding) (mm)		
Segment	**Left**	**Right**	**Average**	**Left**	**Right**	**Average**	**Left**	**Right**	**Average**
L2-L3	0.39 ± 0.31	0.33 ± 0.42	0.36 ± 0.27	−0.39 ± 0.89	−0.60 ± 0.79	−0.50 ± 0.72	0.03 ± 0.80	−0.51 ± 0.46	−0.24 ± 0.44
L3-L4	0.29 ± 0.47	0.26 ± 0.58	0.28 ± 0.49	−0.66 ± 1.22	−0.84 ± 1.23	−0.75 ± 1.17	0.29 ± 0.88	−0.22 ± 0.67	0.03 ± 0.74
L4-L5	0.51 ± 0.47	0.90 ± 0.47	0.70 ± 0.43	−0.86 ± 1.25	−0.88 ± 1.22	−0.87 ± 1.06	−0.13 ± 0.75	0.29 ± 1.03	0.08 ± 0.71
L5-S1	−0.22 ± 0.56	0.13 ± 0.58	−0.04 ± 0.49	1.63 ± 1.13	2.51 ± 1.30	2.07 ± 1.12	0.67 ± 0.75	0.74 ± 0.98	0.70 ± 0.77

Table 2

Segment-specific facet joint translations at the upright standing position with respect to the fully flexed position. Median (confidence interval range based on $\pm CI_{notch}$).

	(a) *X* (facet gap) (mm)			(b) *Y* (SI sliding) (mm)			(c) *Z* (sideways sliding) (mm)		
Segment	**Left**	**Right**	**Average**	**Left**	**Right**	**Average**	**Left**	**Right**	**Average**
L2-L3	0.59 [a] (0.30 – 0.87)	−0.10 [bc] (−0.28 to 0.08)	0.19 [ac] (0.04–0.33)	−5.66 [a] (−6.39 to −4.92)	−6.07 [a] (−6.71 to −5.42)	−5.92 [a] (−6.56 to −5.28)	−0.56 [a] (−0.76 to −0.37)	−0.72 [a] (−0.91 to −0.53)	−0.68 [a] (−0.81 to −0.55)
L3-L4	0.32 [a] (0.17–0.46)	−0.29 [b] (−0.40 to −0.17)	0.03 [c] (−0.07 to 0.12)	−5.97 [a] (−6.58 to −5.36)	−6.06 [a] (−6.59 to −5.52)	−6.34 [a] (−6.91 to −5.78)	−0.60 [a] (−0.84 to −0.36)	−0.65 [a] (−1.15 to −0.14)	−0.73 [a] (−1.12 to −0.34)
L4-L5	0.30 [a] (−0.01 to 0.61)	0.39 [ac] (0.05–0.72)	0.44 [a] (0.23–0.66)	−6.51 [a] (−7.03 to −6.00)	−6.11 [a] (−6.80 to −5.43)	−6.59 [a] (−7.24 to −5.94)	−1.17 [b] (−1.43 to −0.92)	−1.56 [b] (−1.95 to −1.17)	−1.45 [b] (−1.76 to −1.14)
L5-S1	0.45 [a] (0.17–0.74)	0.46 [ac] (0.07–0.86)	0.41 [a] (0.17–0.65)	−3.98 [b] (−4.70 to −3.25)	−3.01 [b] (−3.58 to −2.43)	−3.48 [b] (−4.07 to −2.89)	−1.61 [b] (−2.27 to −0.96)	−1.03 [ab] (−1.50 to −0.57)	−1.63 [b] (−1.95 to −1.30)

Note: Within each component, values with one or more like superscripts (a, b, c, d) across side (left, right, average) or across segment level (L2L3, L3L4, L4L5, L5S1) indicates no significant differences. Dissimilar superscripts indicate significant differences.

Table 3

Load-specific facet joint translations at the flexed position with respect to upright standing position. Median (confidence interval range based on $\pm CI_{notch}$).

	(a) X (facet gap) (mm)			(b) Y (SI sliding) (mm)			(c) Z (sideways sliding) (mm)		
Segment	**Left**	**Right**	**Average**	**Left**	**Right**	**Average**	**Left**	**Right**	**Average**
4.5 kg (10 lb)	0.32 [a] (0.08–0.55)	−0.01 [a] (−0.21 to 0.21)	0.22 [a] (0.05–0.39)	−6.04 [a] (−6.80 to −5.27)	−5.49 [a] (−6.21 to −4.76)	−5.80 [a] (−6.48 to −5.12)	−0.94 [a] (−1.21 to −0.67)	−1.11 [a] (−1.44 to −0.78)	−1.02 [a] (−1.30 to −0.74)
9.1 kg (20 lb)	0.39 [a] (0.16–0.61)	−0.07 [a] (−0.31 to 0.18)	0.19 [a] (0.04–0.35)	−5.72 [a] (−6.56 to −4.88)	−5.59 [a] (−6.44 to −4.75)	−5.54 [a] (−6.34 to −4.74)	−0.69 [a] (−0.94 to −0.43)	−1.07 [a] (−1.51 to −0.63)	−0.96 [a] (−1.26 to −0.66)
13.6 kg (30 lb)	0.34 [a] (0.08–0.60)	−0.06 [a] (−0.32 to 0.19)	0.19 [a] (0.01–0.37)	−5.87 [a] (−6.62 to −5.12)	−5.64 [a] (−6.33 to −4.96)	−5.68 [a] (−6.36 to −5.01)	−0.81 [a] (−1.04 – −0.58)	−0.99 [a] (−1.30 – −0.68)	−0.98 [a] (−1.28 – −0.68)

Note: Within each component, values with one or more like superscripts (a, b, c, d) across side (left, right, average) or across load level (4.5 kg, 9.1 kg, 13.6 kg) indicates no significant differences. Dissimilar superscripts indicate significant differences.

Table 4

Segment-specific coupled lateral bending range of rotation during extension motion. Values are mean and 95% Confidence Intervals $\left(\bar{x} \pm CI_{95}\right)$.

Segment	Coupled lateral bending(°)	Sagittal extension (°)
L2-L3	1.9±1.0	9.9±1.5
L3-L4	1.9±0.5	10.7±1.4
L4-L5	1.5±0.6	12.1±2.0
L5-S1	1.4±0.6	9.6±2.1